Wetting of Hydrophobic Organic Surfaces and Its Implications to Organic Aerosols in the Atmosphere

Yinon Rudich,*,† Ilan Benjamin,‡ Ron Naaman,§ Elan Thomas,† Sofia Trakhtenberg,§ and Rachel Ussyshkin§

Department of Environmental Sciences, Weizmann Institute, Rehovot 76100, Israel, Department of Chemistry, University of California, Santa Cruz, California 95064, and Department of Chemical Physics, Weizmann Institute, Rehovot 76100, Israel

Received: November 30, 1999; In Final Form: March 7, 2000

The interaction between water and organic substances is of extreme importance in physical, biological, and geological chemistries. Understanding the interactions between water and organic interfaces is one of the earliest chemical quandaries. In this research, self-assembled monolayers (SAMs) were used as a tool to investigate the interaction between water molecules and hydrophobic surfaces. Real-time adsorption and desorption kinetics of water on hydrophobic SAM surfaces was monitored using a new type of field effect transistor (FET)-like device called MOCSER (molecular controlled semiconductor resistor) coated with SAMs. A quartz crystal microbalance (QCM) was used as a complementary technique to give an estimate of total water mass adsorbed. It is shown that water adsorption depends on relative humidity and is reversible. The amount of adsorbed water increased with surface corrugation. The measurements suggest that adsorption takes place as small water clusters, originating on irregularities on the surface organic layer. Molecular dynamics simulations were carried out to study the interactions of water and hydrophobic surfaces as well. These simulations also suggest the formation of water microdroplets on hydrophobic surfaces, and indicate a strong correlation between increased surface corrugation and adsorption. This paper examines the possible consequences of these interactions on the properties of organic aerosols in the troposphere.

I. Introduction

The interfacial interactions between water and organic substances receive much attention due to their importance in many fields, among them biology, atmospheric chemistry, and technology (see, for example, refs 1−3). Previously, such interactions were studied both experimentally and theoretically.[4−7] It was proposed that the hydrophobic interface leads to ordering of the water molecules[8] and that the water structure can be perturbed up to few micrometers away from the surfaces.[9] In other studies, the effect of water restructuring around alkyl groups was found to be minimal.[10] Molecular dynamics simulations suggested that cavities could form as a result of the interaction between water and hydrophobic substance.[9,11] Another recent molecular modeling study of water near hydrophobic surfaces has revealed a clathrate hydrate structure.[12] Previous experiments to measure water adsorption on organic surfaces utilized a variety of techniques such as infrared spectroscopy, temperature-programmed desorption (TPD), and quartz crystal microbalance (QCM).[12−15] Despite the wealth of studies, many aspects regarding the mechanism of water adsorption on hydrophobic surfaces are still not well-known.

Recently, a new type of field effect transistor (FET) was developed. The MOCSER (molecular controlled semiconductor resistor) is a special FET, designed for measuring minor changes in its surface charge density. In contrast to the common FET, which has three electrodes (gate, source, and drain) the MOCSER has only a source and drain. When a voltage is applied between the source and drain electrodes, current flows through the MOCSER's active layer. Adsorption of molecules on the MOCSER surface affects the charge distribution on the device surface, changing the surface electrostatic potential. The adsorbed molecules function as the "gate" that modulates the current. The current can either increase or decrease depending on the specific electronic interactions involved, and the kinetics of adsorption on MOCSER surface can be studied by monitoring the current. It was found that the change in the current is proportional to the surface coverage by the adsorbed species.[16] In the present study, MOCSER surfaces were covered with organic self-assembled monolayers (SAMs) and adsorption of water was measured as a function of the SAM surface properties. While MOCSER is sensitive only to molecules in contact with the surface, QCM measured the total mass adsorbed. Therefore, simultaneous measurements by MOCSER and QCM were employed for studying water adsorption kinetics on organic hydrophobic surfaces by conducting real-time measurements of both surface coverage and mass change.

Molecular dynamics simulations were performed in order to understand the interactions between a hydrophobic organic layer with gas-phase water molecules. Theoretical studies of water next to surfaces have a long history, and we refer the reader to several recent reviews of this topic in the general context of liquids at interfaces.[17,18] It was realized early on that the behavior of water next to any surface is a result of the delicate balance between long-range interactions, the short-range water−surface atoms interactions, and the driving force for water molecules to keep their hydrogen bonds network intact. Although the short-range interactions are not expected to depend significantly on the morphology of the surface, the hydrogen bonding network is quite sensitive to this aspect, as has been demonstrated by recent molecular dynamics simulations where the issue of

† Department of Environmental Sciences.
‡ Department of Chemistry.
§ Department of Chemical Physics.

10.1021/jp994203p CCC: $19.00
Published on Web 05/16/2000

hydrogen bonding at interfaces is directly examined.[6,19] In the present work, as a complementary study to the experimental investigations, we look more specifically at the collective behavior of a monolayer of adsorbed water molecules on hydrocarbon surfaces of different, well-defined corrugation. This part of the work is closely related to molecular dynamics investigations by Hautman and Klein,[20] who examined the difference in wetability between hydrophobic and hydrophilic surfaces. Using these tools, we have developed a geometrical model for the interaction of water with these organic surfaces, which is dependent on the surface morphology. Discussion of the implication of this model to the understanding of the atmospheric properties of organic aerosols is presented.

II. Wettability of Hydrophobic Surfaces

a. Experimental Details. The design and properties of the MOCSER have been described previously, and they will not be discussed here.[16,21,22] Both the MOCSER and QCM were covered with 100−200 nm of plasma-deposited SiO_2, which is the substrate on which organic monolayers bind to the surface. By coating the active surface of these devices with SAM, hydrophobic surfaces with known qualities (chain length, packing, surface roughness) are made. Several different types of monolayers were adsorbed, with variable chain lengths. They include octadecyltrichlorosilane (OTS), dodecyltrichlorosilane (DTS), octyltrichlorosilane (OcTS), octenyltrichlorosilane (OcEnTS), methyltrichlorosilane (MTS), and mixed monolayers of OcTS/DTS and DTS/OTS. The technique of self-assembly is well-known and is described elsewhere.[23,24] As confirmation of monolayer quality, the contact angle formed by a water droplet on the surface was measured. Additional qualitative information was obtained from the infrared spectra of the films, measured in the direct adsorption mode on the Bruker IFS-66 spectrometer.

The QCM and MOCSER devices were placed in a dark glass chamber with a dry nitrogen atmosphere. Variable humidities were generated by a two-stream nitrogen flow system. One stream flowed through a deionized water bubbler to create a near saturated state, while the other remained dry. By controlling the ratio of these two flows into the chamber, humidity could be easily regulated. Fast mixing of humid and dry air in the chamber was achieved by conditioning the system with humid air prior to exposure of the organic surface. The saturated flow was generated by bubbling N_2 through a reservoir of deionized water and was calibrated with a standard RH measurement instrument (2% accuracy at RH < 97%). In this work, the term 100% RH will refer to all conditions in which humidities above 97% were used. All the measurements were taken at 1 atm and 25 °C. Current from the MOCSER was measured using a Keithley model 487-picoammeter/voltage source. Changes in the QCM resonance frequency were simultaneously measured using a model TM-100 thickness monitor (R. D. Mathis Co.). Experiments were performed simultaneously for MOCSER and QCM, and concurrent real-time data were collected.

b. Results and Discussion. The normalized response of the MOCSER to humidity is displayed in Figure 1. The current through the device increases as water adsorbs to the surface, until desorption and adsorption from the surface reaches equilibrium. The current at equilibrium varies with relative humidity (RH) and is proportional to the coverage of water in contact with the surface. As the water is turned off, water desorbs from the surface and the current slowly returns to its original value. The adsorption curves were normalized

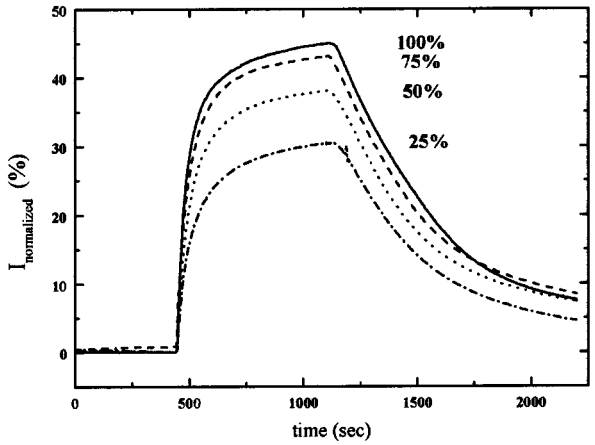

Figure 1. The normalized current through the MOCSER covered with OTS. During the measurements constant voltage of 0.05 V was applied. In each measurement nitrogen containing water vapor of various concentrations was inserted to the chamber at $t = 450$ s and removed at $t = 1120$ s. The numbers near the curves correspond to the relative humidity of the moist nitrogen.

according to

$$I_{\text{norm}}(t) = \left(\frac{I(t)}{I_{\text{initial}}} - 1\right)100\% \tag{1}$$

Equation 1 represents a percentage change in the MOCSER current with exposure to humidity.

The adsorption measured by the MOCSER was analyzed using the Langmuir isotherm.[25] In the Langmuir model, the ratio between the number of occupied adsorption sites and the total number of sites is defined as θ which is given by

$$\theta = \frac{KC}{1 + KC} \tag{2}$$

where $K = k_A/k_D$ is the adsorption equilibrium constant and C is the water vapor concentration. Setting $\theta = I_{\text{norm}}/I^{\infty}_{\text{norm}}$($I_{\text{norm}}$ is the normalized current at the specific coverage and I^{∞}_{norm} is the normalized current corresponding to 100% coverage) eq 2 can be rearranged into

$$\frac{C}{I_{\text{norm}}} = \frac{C}{I^{\infty}_{\text{norm}}} + \frac{1}{KI^{\infty}_{\text{norm}}} \tag{3}$$

A plot of C/I_{norm} versus C yields a straight line with a slope of $(I^{\infty}_{\text{norm}})^{-1}$ and an intercept of $(KI^{\infty}_{\text{norm}})^{-1}$. The ratio of slope to intercept yields the adsorption equilibrium constant K (in units of L/mmol). A plot of eq 3 for OTS is shown in Figure 2A. The equilibrium constant determined for OTS is $K = 3.4 \pm 1.6$ L/mmol. This equilibrium constant corresponds to about 70% coverage of the available surface adsorption sites at 50% relative humidity. Equilibrium constants for the other organic surfaces measured were within the same order of magnitude, with the highest being 6.1 ± 3.4 L/mmol for the OcTS monolayer.

Figure 2B presents the I_{norm} as a function of water vapor concentration. As predicted by the Langmuir model, this presentation does not have a linear dependence, since linear dependence between the amount of the adsorbed species on the surface and its concentration is expected only in cases where adsorption is not limited by the number of sites. This happens when $KC \ll 1$ and therefore $\theta = KC$.

The effect of substrate corrugation on the equilibrium constant was investigated using wettability of water (contact angle, CA)

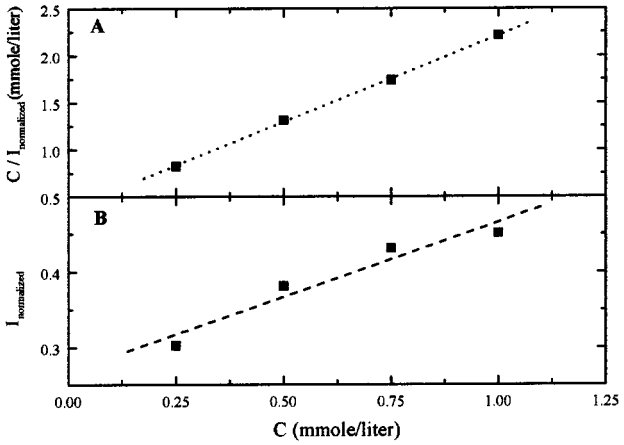

Figure 2. (A) The ratio between the water vapor concentration to the normalized current through the MOCSER at saturation, as a function of the water vapor concentration. The dotted line is a linear fit to the experimental results. (B) I_{norm} at saturation, as a function of the water vapor concentration. The dashed line is a linear fit to the experimental results.

TABLE 1: Water Contact Angles and Langmuir Equilibrium Constants (*K*) for the Surfaces Examined

film	advancing CA (deg)	receeding CA (deg)	hysteresis (deg)	*K* (L/mmol)	θ at 50% RH
C_{18}(OTS)	116	111	5 ± 2	3.4 ± 1.6	0.6
C_{12}(DTS)	115	108	7 ± 2	3.0 ± 1.6	0.6
C_8(OcTS)	114	103	9 ± 2	6.1 ± 3.4	0.8
$C_8^=$(OcEnTs)	97	89	8 ± 2	5.2 ± 2.3	0.7
C_{18}/C_{12}(OTS/DTS)	116	111	5 ± 2	2.3 ± 1.6	0.5

measurements that provide information on the ordering of the organic film.[26,23] More ordered films have a larger advancing contact angle and smaller difference between the advancing and the receding contact angles (hysteresis). In Table 1, the results of wettability and water adsorption measurements are summarized.

Adsorption of water on the organic surface induces an increase in the MOCSER current. In contrast, the MOCSER current decreases due to exposure to molecular oxygen. This behavior results from different electronic interaction between the adsorbate and the organic molecules on the surface. Oxygen affects the current independently of water presence on the surface. The response to oxygen, which is observed with and without water present, can be explained if the surface is only partially covered by water, so that O_2 can reach the surface. The same phenomena was observed also for DTS and OcEnTS surfaces with up to 100% RH.

Since the MOCSER is sensitive only to the first adsorption layer, the absolute amount of water on the surface cannot be obtained. Therefore, an independent technique that is sensitive to the total mass, such as quartz crystal microbalance (QCM), is used. The QCM response, given in units of layer thickness, was calibrated by measuring the thickness difference of a quartz crystal covered by two different SAMs of known length difference: OTS and DTS. There is an approximate 10 Å difference in the lengths of these chains. The amount of adsorbed water on OTS monolayer was calculated to be larger than the amount needed to complete one monolayer of water. Because of difficulties in quantitative measurements of liquid film adsorption by microbalance techniques[15] and the variability of the surfaces, the exact amount of adsorbed water on the surface could not be determined. An upper bound for the amounts of adsorbed water is the equivalent of up to 10 monolayers-equivalents of water on the roughest surface. Substantially higher

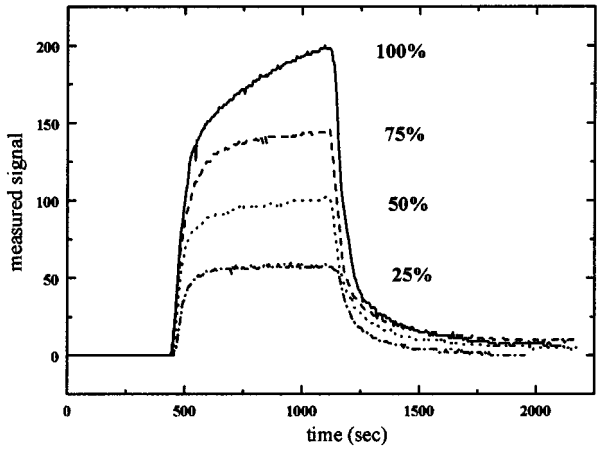

Figure 3. The thickness of the layer of water adsorbed on OTS measured by QCM thickness monitor. The measurements were done simultaneously with measuring of the current through the MOCSER covered with OTS. The numbers near the curves correspond to relative humidity of the moist nitrogen.

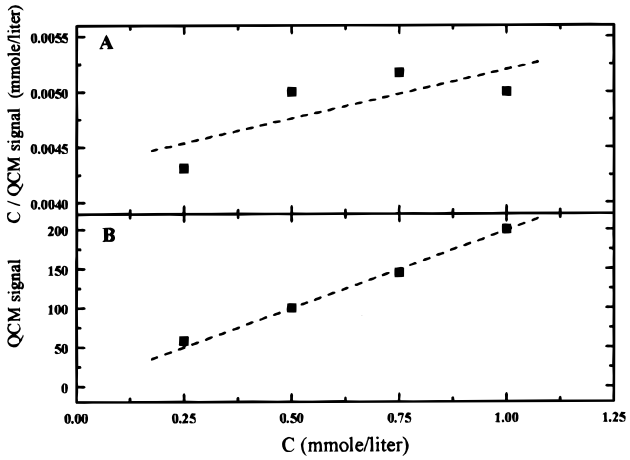

Figure 4. (A) The ratio between the water vapor concentration to the thickness of the adsorbed water layer measured by QCM, at saturation, as a function of the water vapor concentration. The dashed line is a linear fit to the experimental results. (B) Thickness of the adsorbed water layer measured by QCM, at saturation, as a function of the water vapor concentration. The dashed line is a linear fit to the experimental results.

water uptake was measured on MTS surfaces, known to be less ordered than OTS and DTS. This observation is also consistent with the notion that higher ordering leads to lower water adsorption.

Figure 3 shows the mass of water adsorbed on the OTS as a function of time, measured by the QCM, for several concentrations of water vapor. It can be clearly seen that the kinetics of water adsorption on OTS is different for MOCSER and QCM measurements. The differences become more apparent when Figure 2A is compared to Figure 4A, where the kinetics of water adsorption on QCM is fitted to the Langmuir model. A nonlinear dependence between water vapor concentration and the amount of adsorbed water is apparent. Forcing a Langmuir model fit (with a large standard error) yields a $K = 0.2$ L/mmol. This equates to 10% water coverage of available adsorption sites at 50% relative humidity. However, the QCM signal is directly proportional to water vapor concentration (Figure 4B). Comparison between the MOCSER and QCM results and their interpretation are summarized in the Table 2.

The MOCSER and QCM measurements provide complementary pictures to the adsorption of water onto hydrophobic

TABLE 2: Adsorption of Water and Oxygen on OTS Surface Measured by MOCSER and QCM Techniques

	MOCSER	QCM	conclusions
Langmuir kinetics ($\theta = KC/1 + KC$)	excellent fit	poor fit	MOCSER: independent molecular adsorption on hydrophilic sites.
$K = k_A/k_D$	3.4 ± 1.7 L/mmol	0.2 ± 0.1 L/mmol	QCM: water equivalent to a few molecular layers reside on the surface.
θ at 50% RH	(60 ± 12) %	(9 ± 4) %	
"linear" kinetics	does not fit	fits well	MOCSER: adsorption is limited by the number of surface sites. Does not measure the second layer formation. QCM: adsorption is not limited by the number of surface sites. Adsorption on adsorbed water.
coadsorption of water and oxygen	Independent of }water adsorption	QCM does not sense the O_2 adsorption	MOCSER: O_2 and water adsorb to different sites. Water does not cover the entire surface. QCM: the total mass of adsorbed water is significantly larger than the total mass of adsorbed O_2. Therefore, lack of sensitivity for O_2 uptake.

surfaces. The results suggest that water initially adsorbs at imperfections on the monolayer that are situated at a relatively large distance one from another, and therefore the adsorption of water molecules on one site is independent of other sites. Since the MOCSER does not sense the adsorption of additional water layers on top of the first one, the measured coverage is always less than a monolayer. This explains the nearly Langmuir kinetics of the adsorption process, as measured by the MOCSER. Of course, water adsorption on hydrophobic surfaces is not inherently expected to follow the Langmuir mechanism. This is clearly demonstrated by the QCM measurements that show water adsorption beyond the first adsorption layer. Because of the hydrophobicity of OTS and the strong water-water interactions, we propose that the adsorbed water will form small surface-bound microdroplets. These droplets do not cover the whole surface area, as is evident from the coadsorption of O_2 and water experiments. Hence, the kinetics of the adsorption of the first water "layer" directly on the OTS surface is screened by the kinetics of water-on-water adsorption. The QCM measurements also show that the amount of adsorbed water is proportional to the water vapor concentration which is the case when water adsorption is not limited by the number of surface adsorption sites. This observation supports the model that water molecules adsorb on previously adsorbed water molecules, hence the adsorption of each additional molecule does not affect the number of available adsorption sites.

III. Molecular Dynamics Simulations

a. System and Potential Energy Functions. The system modeled includes 100 hydrocarbon molecules covalently attached on one end to the Si atoms of the silica surface. We assume an underlying square symmetric lattice with a distance of 4.3 Å between the neighboring Si atoms. This results in a 43 Å × 43 Å surface. Two systems are constructed: system A, which is made of 100 $C_{18}H_{38}$ molecules, and system B, which is made of 50 $C_{18}H_{38}$ molecules and 50 $C_{22}H_{46}$ molecules. In system B, the molecules of the two types are bonded to the surface in a random order, which is consistent with the fact that experimentally no self-aggregation of the two different types of the molecules occurs.

Each hydrocarbon molecule is modeled as a chain of CH_2 groups treated as united atoms of mass 14 terminated by a CH_3 group which is modeled as a united atom of mass 15 (i.e., no explicit hydrogen atoms are used). Each one of these united atoms is interacting with united atoms from different chains via a Lennard-Jones potential:

$$u_{ij}(r) = 4\epsilon_{ij}\left[\left(\frac{\sigma_{ij}}{r}\right)^{12} - \left(\frac{\sigma_{ij}}{r}\right)^{6}\right] \quad (3)$$

where r is the distance between atoms i and j. In this expression, the Lennard-Jones parameters σ_{ij} and ϵ_{ij} are computed from the standard parameters of the CH_2 and CH_3 groups, using the relations[27]

$$\epsilon_{ij} = \sqrt{\epsilon_i \epsilon_j}, \quad \sigma_{ij} = (\sigma_i + \sigma_j)/2 \quad (4)$$

where ϵ_i and σ_i are the Lennard-Jones parameters of the united atom of the type i. We take $\sigma_{CH_2} = \sigma_{CH_3} = 3.905$ Å and $\epsilon_{CH_2} = 0.118$ kcal/mol, $\epsilon_{CH_3} = 0.175$ kcal/mol. The intermolecular interactions are switched smoothly to zero[28] when r is in the range between 19.5 and 21.5 Å. Each of the hydrocarbon molecules is fully flexible. The intramolecular potential includes harmonic stretching and bending terms, a standard three-term Fourier series for the torsional energy[29] (defined between every four consecutive carbon atoms) and nonbonded interactions between two atomic centers separated by three or more bonds. The harmonic force constants, the torsional parameters, and the equilibrium bond length and bond angles are taken from the Amber force field[30] and Jorgensen's TIPS parameters.[31] The intramolecular nonbonded interactions are modeled using the Lennard-Jones potential with parameters $\sigma = 4.0$ Å and $\epsilon = 0.1$ kcal/mol. The interaction is scaled down by a factor of 2 for the 1,4 carbon atoms in each chain.[29]

The water potential energy function is based on the SPC model,[32] including the spectroscopic intramolecular potential of Kuchitsu and Morino.[33] This flexible model of water has been shown to give a reasonable representation of bulk and interfacial water properties.[6] The water−hydrocarbon chain interactions are also modeled using the Lennard-Jones potential and the mixing rule (eq 4).

b. Procedure and Results. Following the construction of the two systems, a 1 ns molecular dynamics trajectory is run in order to obtain the equilibrium structure of the chains on the surface. We expect that the system made of only C_{18} chains will give rise to a smooth surface, and the system made of 50% C_{18}/C_{22} mixtures will give rise to a very rough surface.

The top panel of Figure 5 shows the orientational probability density distribution function $P(\theta)$ of the angle θ between the end-to-end carbon atoms and the normal to the surface. The distribution is normalized such that $\int_0^\pi P(\theta) \sin\theta \, d\theta = 1$. The solid line, which corresponds to the smooth homogeneous surface, shows that for this system the chains are mostly perpendicular to the surface. The dashed line, which corresponds to the mixed system, shows that the chains are tilted on average by an angle of 13° to the normal. These results are in agreement with experiments.

The middle panel of Figure 5 gives the probability distribution of the torsional angle ϕ defined by the top four carbon atoms of each chain. The fact that the distribution peaks at 180° shows

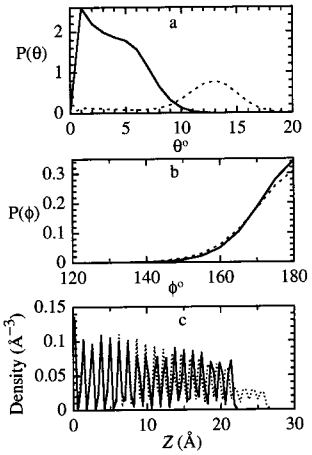

Figure 5. The equilibrium structure of the (dashed line) C_{18}/C_{22} and the (solid line) C_{18} hydrocarbon chain systems. (a) The probability density for the angle between the end-to-end carbon atoms and the normal to the interface. (b) The probability distribution of the end-chain torsional angle. (c) The carbon atom density profile as a function of the *Z* distance from the silica surface.

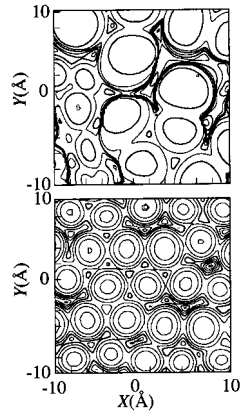

Figure 6. Potential energy contour plots for the binding energy of a single water molecule on the (top) rough (C_{18}/C_{22}) and (bottom) smooth (C_{18}) surfaces. The contour lines correspond to a separation of 0.5 kcal/mol.

that most of the chains are in the trans conformation. The small difference between the two surfaces (solid line, the smooth all-C_{18} surface; dashed line, the mixed rough surface) is consistent with more gauche defects in the mixed system, as expected.

The bottom panel of Figure 5 shows the carbon atom density profile as a function of the distance from the silica surface. The marked regular oscillations are consistent with the high-density solid-like packing of the chain near the solid surface in both systems. However, near the top of the chains the mixed system shows considerable irregular oscillations, which are more consistent with a liquid-like density profile. Here again, the mixed layer (dashed line) is more irregular than the all C_{18} surface (solid line).

Additional information about the structure of the surface that is particularly relevant to the wetting studies can be obtained by computing the binding energy of a single water molecule on the surface. This is given as a contour plot in Figure 6, which shows a 10 Å × 10 Å section of the surface of each system. The top panel corresponds to the mixed C_{18}/C_{22} system and the bottom panel to the homogeneous C_{18} system. The contour lines represent energies that are separated by 0.5 kcal/mol. It is clear that the surface of the mixed system is highly disordered compared with the much more ordered surface of the homogeneous system. The rough surface is also characterized by larger binding energies. For example, in the surfaces given in

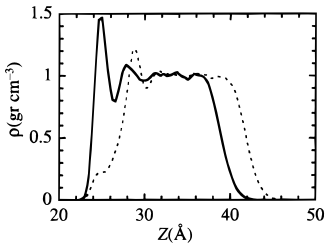

Figure 7. The water density profile as a function of the distance from the surface at $T = 300$ K. Ordered C_{18} surface, solid line; rough surface, dotted line.

Figure 6, the lowest minimum on the rough surface is at −2.40 kcal/mol compared with only −1.23 kcal/mol on the smooth surface. The sites of lowest binding energy correspond to locations where a single C_{18} chain is surrounded mainly by C_{22} molecules, so that a water molecule is interacting with a large number of carbon atoms from the sides as well as from below. Note also that the rough surface has a larger fraction of regions where the water binding energy is not so negative. These correspond to locations of C_{22} chains that are not densely packed (due to a number of shorter C_{18} molecules nearby). These facts will manifest themselves in the wetting properties of these surfaces, as will be shown below.

Another way to demonstrate the different structure of the two surfaces as seen by water molecules is to examine the density profile of several water layers in contact with the surface. This is shown in Figure 7, where *Z* corresponds to the distance from the underlying silica surface. There are 970 water molecules in this simulation, which corresponds to approximately five layers. The water density next to the smooth surface is very similar to the one expected from water next to a flat solid wall, whereas the water next to the rough surface shows a tail closer to the surface than the first main peak. This represents water molecules that interact with the shorter C_{18} chains and thus "penetrate" the surface. Because of the high density of the surface, there are no water molecules closer to the surface than the top carbon atom of the short chains. The water molecules far from the organic surface were allowed to establish equilibrium with the vapor phase, which is consistent with the experimental setup. This can be seen from the tail of the density profile near $Z =$ 45 Å.

We finally discuss the wetting properties of the two surfaces considered above, which we will refer to as the rough (the C_{18}/C_{22} mixture) and the smooth (pure C_{18} chains) surface. We start with a monolayer of water (196 molecules) adsorbed on each of the two surfaces, and we follow the system for 1 ns. The interaction energy of water with the surface is given in Figure 8 as a function of time. The two systems start from nearly the same value of this interaction energy (about −70 to −80 kcal/mol). However, after 1 ns the interaction energy of the water monolayer adsorbed on the smooth surface (panel a) is only −30 kcal /mol, whereas the water monolayer on the rough surface still interacts strongly with the surface (average interaction energy of −50 kcal/mol). An examination of the structure of the system reveals that the water monolayer on the smooth surface forms a drop (a de-wetting transition) whose interaction with the surface is much less than that of the monolayer. There is a corresponding increase in the water−water hydrogen bonding energy: the average nonbonded water energy changes from −7.5 to −10.7 kcal/mol (the value that is almost identical to that of bulk water). In contrast, the water on the rough surface remains largely in contact with most of the surface. There are regions where the water forms small drops (a few tens of molecules), and so the average water−water nonbonded energy

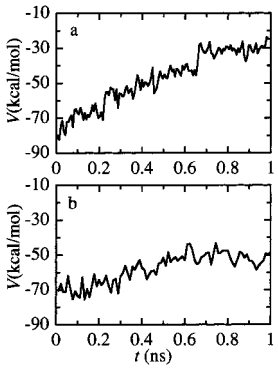

Figure 8. The water−surface interaction energy as a function of time, starting from monolayer coverage of water on the (top part) smooth and (bottom part) rough surfaces.

also goes down from −7.5 to −8.8 kcal/mol, but in this system the water is clearly wetting the surface. A picture of the simulation for rough and smooth surfaces demonstrating the wetting of the two surfaces is shown in Figure 9. A side view of the water-surface interaction is shown in Figure 10. Figure 10 clearly shows the effect of water penetration into the surface and how it affects water structure near hydrophobic surfaces.

In conclusion, the molecular dynamics simulations underscore the relationship between the wetting properties and the microscopic structure and potential energy of the organic surfaces, in agreement with the experiments.

IV. Summary of Results

Both the simulations and measurements show that the corrugation of the hydrophobic surface has an important effect on how water arranges near a hydrophobic surface. In the case of a smooth hydrophobic surface, water minimizes its interaction with the surface and forms a droplet, keeping minimal contact with the surface. In the case of a rough surface, water penetrates through structural irregularities on the surface. This configuration allows the water molecules to interact more with the surface and the surrounding chains, and therefore stay on it. This initial stage is followed by formation of bonds with more water molecules. This causes wetting of the surface and formation of small micro droplets on the surface. These results are depicted in Figures 9 and 10. They are completely consistent with the conclusions drawn based on the experiments.

The present measurements and simulations suggest that water adsorption is intimately related to surface corrugation. Water molecules have a larger probability of binding to structural

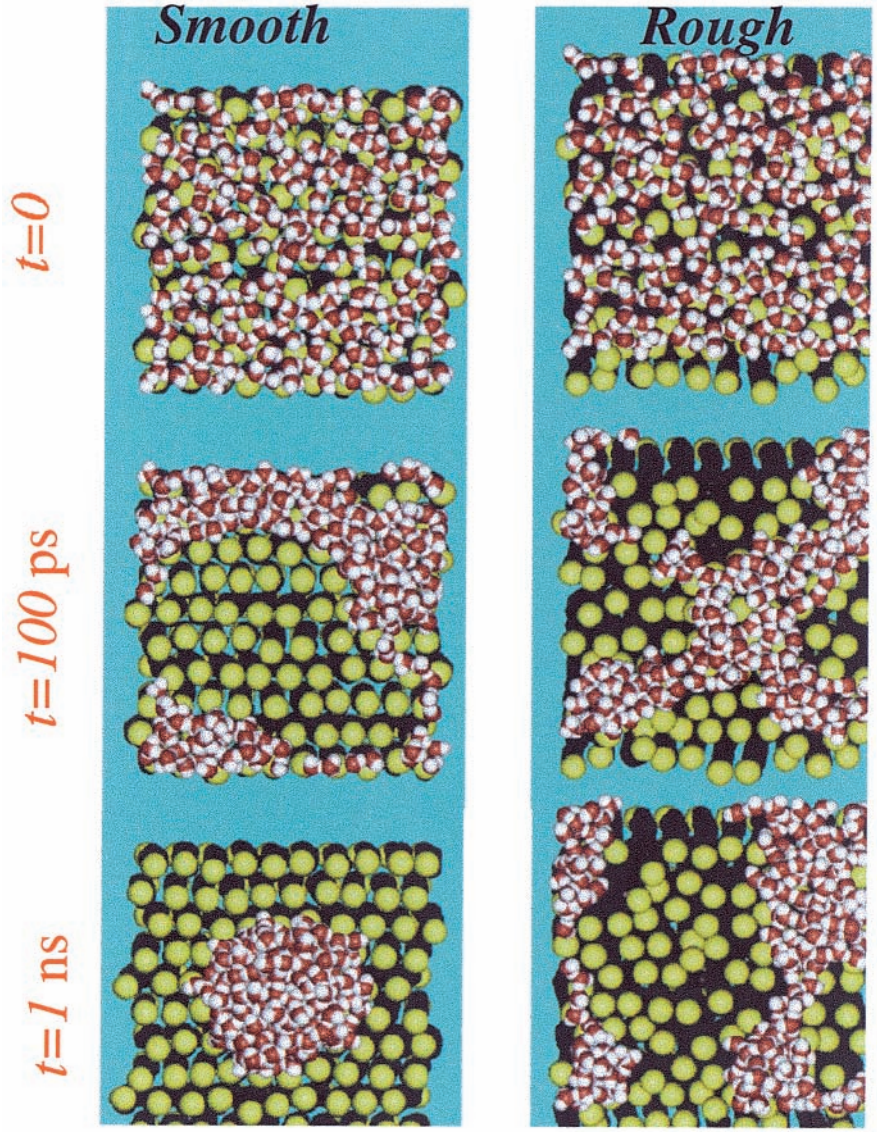

Figure 9. Time dependent molecular dynamics simulation of water in the proximity of a hydrophobic surface. It can be seen that while in a smooth surface (left part) water molecules (red and white) form a droplet on the surface (yellow), they clearly wet the rough surface (right part).

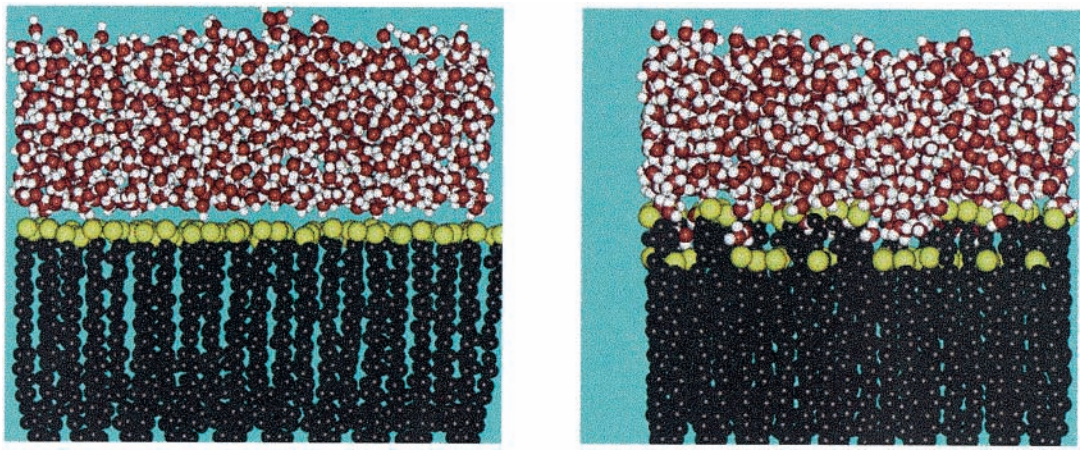

Figure 10. Side view of the structure of water close to a hydrophobic surface calculated by molecular dynamics simulation, showing the effect of roughness. The left panel shows that water minimizes contact with a smooth surface, while water molecules penetrate into a rough surface and enable its wetting.

irregularities on the hydrophobic organic surfaces, even when the surface is considered very smooth. The initial surface-bound water molecules enable further accumulation of water until small clusters or microdroplets form on the surface. The adsorption is reversible, in equilibrium with the ambient humidity. The morphology of hydrophobic surfaces determines the amount of water that can bind to the surface. This conceptual model of water binding resembles the phenomenon observed for some other inorganic systems. For example, adsorption of water on the surface of salts is greatly enhanced by surface defects and atomic steps,[34−38] while corrosion by sulfuric acid also proceeds via formation of surface defects.[39] Surface morphology also plays a role in determining the structure of ice forming on hydrophobic surfaces[40] and in water adsorption on mica.[41] Finally, adsorption of water on activated carbon also follows a similar mechanism: Water sticks to sites on edges of the graphene layers. As the water vapor pressure is increased, the adsorption increases by the formation of clusters of water molecules located around the primary adsorption sites. The distance between the primary sites is large compared with the water clusters. This mechanism was confirmed both experimental and by molecular dynamics simulations.[42,43]

V. Implications to Atmospheric Organic Aerosols

Aerosols are prevalent in the atmosphere and are recognized to play important roles in climate through their interaction with solar and terrestrial radiation, as well as by affecting cloud properties and by providing a medium for chemical reactions. Understanding the interactions between atmospheric aerosol surfaces and water is necessary for identifying their role in affecting cloud properties, their optical properties and their heterogeneous atmospheric processes.[44] The chemical composition is important in determining the aerosol's optical and chemical properties.[45−48] Organic compounds from biogenic and anthropogenic sources can form organic aerosols, either through their direct emissions or by chemical reactions within the atmosphere. Field measurements have demonstrated that organic aerosols are common throughout the atmosphere, in both continental and marine environments.[49−51] Although usually considered insoluble, organic aerosols have been shown to be large contribution to cloud condensation nuclei (CCN).[52] Recently, it has been shown that aerosols coated by both hydrophobic and hydrophilic organic layer may act as CCN even at normal atmospheric saturation conditions.[53]

Organic aerosols are usually divided into primary and secondary aerosols. Primary organic matter is emitted directly to the atmosphere as particles by anthropogenic sources such as combustion and cooking, or by biogenic sources. These particles are usually composed of low vapor pressure, high molecular weight hydrophobic substances. The secondary organic aerosol form by condensation of low vapor pressure organics produced in the atmosphere by photodegradation of higher vapor pressure organics. The secondary aerosols contain more oxygenated compounds and therefore can be more hydrophilic. In addition to these aerosol types, it was suggested that fresh sea-salt aerosols contain hydrophobic organic matter (such as fatty acids and humic substance) that is removed from the ocean surface by the action of breaking waves. Subsequent processing by atmospherics oxidants and radicals can transform the hydrophobic organic aerosols to more hydrophilic ones.[54]

We regard the organic surfaces used in the present experimental and theoretical study as model systems for understanding the interaction of water with hydrophobic surfaces in general, and the properties of atmospheric hydrophobic organic surfaces, such as fresh primary and organic coated sea-salt aerosols, in particular. Obviously, in comparison to real hydrophobic atmospheric surfaces, the studied surfaces are more ordered and uniform than any natural system. Therefore, the findings of this study can only be treated as a lower limit to the interactions expected in the atmosphere. We implement the findings of our study to the development of a conceptual framework for understanding the interactions of water with hydrophobic organic surfaces.

The lower right-hand side part of Figure 9 shows an animation of how we envision atmospheric hydrophobic organic surfaces. Since the aerosol surface is rough, water can bind to kinks and jogs on the surface, providing "nucleation" centers for further water adsorption. The surface is clearly "wet", and partially covered by the surface-bound water. Processes that can occur within this layer will affect the aerosol properties (mass, optical, chemical) and therfore its atmospheric lifetime.

Interfacial water, adsorbed on the surface of organic aerosols, even if the volume fraction of water is small, may play important roles in the chemistry and physics of the aerosols. Some atmospheric gases are very soluble in cloudwater.[3] This suggests that soluble gaseous species may be concentrated within the surface-bound water droplets. The interfacial water droplets may become a medium for chemical reactions that are either slow or not possible in the gas phase, such as hydrolysis, ionization,

and oxidation. Examples may be hydrolysis of species such as HNO_3 and N_2O as well as sulfur oxidation. Such processes can change the properties of the hydrophobic surfaces causing them to be more hydrophilic. However, treatment of chemical reactions in these small volumes is not well developed at present.[55]

Interfacial water on organic aerosols may also be of importance to the growth process of secondary aerosols. Several studies have postulated the existence of a quasi-liquid layer on the surfaces of organic aerosols.[56−58] This layer will have very distinct uptake properties, different from those of the (liquid-like) organic component. This may explain the effect of relative humidity on the growth of secondary organic aerosols. Because the adsorption is reversible, the amount of surface-bound water will change with the ambient relative humidity and different parts of the surface will be covered by water at different times.

Aerosols directly effect climate by absorbing and reflecting solar and terrestrial radiation and indirectly by modifying clouds properties. The microdroplets on the surface of organic aerosols may change their optical properties, their chemical properties and their atmospheric lifetime, and through this also their climatic effects.

VI. Conclusions

Because of the weak interactions between water and hydrophobic surfaces every small change in the surface morphology, due to corrugation, can significantly affect the structure of the adsorbed layer. It was found that, at room temperature, the adsorption of water occurs mainly on surface defects.

Water adsorption on SAMs at room temperature and at atmospheric pressure was studied simultaneously by two complementary experimental techniques. The results of these two types of measurements were compared. Water adsorption was found to be reversible and dependent on the relative humidity. Adsorption kinetics measured by MOCSER, which is sensitive to the first adsorbed water layer, resembles Langmuir behavior. The other method (QCM), which is sensitive to the total amount of adsorbed water, shows that the adsorption is non-Langmuir and the amount of adsorbed water is proportional to the concentration of water vapor in the atmosphere. It was also shown that the surface coverage is not complete. A model that is consistent with both findings suggests that water adsorbs as small droplets mainly on imperfections or structural defects on the organic layer. The molecular dynamics simulations underscore the relationship between the wetting properties and the microscopic structure and potential energy of the organic surfaces. The simulation results are in excellent agreement with this model. Finally, we suggest using this model for understanding the interactions of primary organic aerosols with water vapor.

References and Notes

(1) Wang, R.; Sakai, N.; Fujishima, A.; Watanabe, T.; Hashimoto, K. *J. Phys. Chem. B* **1999**, *103* (12), 2188.

(2) Gavish, M.; Wang, J. L.; Eisenstein, M.; Lahav, M.; Leiserowitz, L. *Science* **1992**, *256* (5058), 815.

(3) Ravishankara, A. R. *Science* **1997**, *276* (5315), 1058.

(4) Barziv, R.; Safran, S. A. *Langmuir* **1993**, *9* (11), 2786.

(5) Benjamin, I. *Chem. Rev.* **1996**, *96* (4), 1449.

(6) Benjamin, I. Molecular Dynamics Methods for Studying Liquid Interfacial Phenomena. In *Modern Methods for Multidimensional Dynamics Computations in Chemistry*; Thompson, D. L., Ed.; World Scientific: Singapore, 1998; p 101.

(7) Berezin, G. I.; Vartapetyan, R. S.; Voloshchuk, A. M.; Petukhova, G. A.; Polyakov, N. S. *Russ. Chem. Bull.* **1998**, *47* (10), 1879.

(8) Frank, H. S.; Evans, M. W. *J. Chem. Phys.* **1945**, *13*, 507.

(9) Drost-Hansen, W. *J. Colloid Interface Sci.* **1978**, *58*, 251.

(10) Turner, J.; Soper, A. K. *J. Chem. Phys.* **1994**, *101*, 6116.

(11) Madan, B.; Lee, B. *Biophys. Chem.* **1994**, *51* (2−3), 279.

(12) Head-Gordon, T. *Proc. Natl. Acad. Sci. U.S.A.* **1995**, *92*, 8308.

(13) Masuda, H. *J. Jpn. Inst. Met.* **1998**, *62* (10), 961.

(14) Yano, K.; Bornscheuer, U. T.; Schmid, R. D.; Yoshitake, H.; Ji, H. S.; Ikebukuro, K.; Masuda, Y.; Karube, I. *Biosens. Bioelectron.* **1998**, *13* (3−4), 397.

(15) Rodahl, M.; Kasemo, B. *Sens. Actuators* **1996**, *54* (1−3), 448.

(16) Vilan, A.; Ussyshkin, R.; Gartsman, K.; Cahen, D.; Naaman, R.; Shanzer, A. *J. Phys. Chem. B* **1998**, *102* (18), 3307.

(17) Croxton, C. A., Ed. *Fluid Interfacial Phenomena*; Wiley: New York, 1986.

(18) Israelachvili, J. N. *Intermolecular and Surfaces Forces*; Academic Press: London, 1992.

(19) Pohorille, A.; Wilson, M. A. *J. Mol. Struct. (THEOCHEM)* **1993**, *103* (3), 271.

(20) Hautman, J.; Klein, M. L. *Phys. Rev. Lett.* **1991**, *67* (13), 1763.

(21) Gartsman, K.; Cahen, D.; Kadyshevitch, A.; Libman, J.; Moav, T.; Naaman, R.; Shanzer, A.; Umansky, V.; Vilan, A. *Chem. Phys. Lett.* **1998**, *283* (5−6), 301.

(22) Thomas, E.; Rudich, Y.; Trakhtenberg, S.; Ussyshkin, R. *J. Geophys. Res.* **1999**, *104* (D13), 16053.

(23) Ulman, A. *An Introduction to Ultrathin Organic Films: From Langmuir−Blodgett to Self-Assembly*; Academic: San Diego, California, 1991.

(24) Sagiv, J. *J. Am. Chem. Soc.* **1980**, *102*, 92.

(25) Atkins, P. W. *Physical Chemistry*, 5th ed.; Oxford University Press: New York, 1995.

(26) Wasserman, S. R.; Tao, Y. T.; Whitesides, G. M. *Langmuir* **1989**, *5* (4), 1074.

(27) Hansen, J.-P.; McDonald, I. R. *Theory of Simple Liquids*; Academic: London, 1986.

(28) Allen, M. P.; Tildesley, D. J. *Computer Simulation of Liquids*; Clarendon: Oxford, 1987.

(29) Burket, U.; Allinger, N. L. *Molecular Mechanics*; American Chemical Society: Washington, 1982.

(30) Weiner, S. J.; Kollman, P. A.; Nguyen, D. T.; Case, D. A. *J. Comput. Chem.* **1986**, *7*, 230.

(31) Jorgensen, W. L. *J. Am. Chem. Soc.* **1981**, *103*, 335.

(32) Berendsen, H. J. C.; Postma, J. P. M.; Gunsteren, W. F. V.; Hermans, J. *Intermolecular Forces*; D. Reidel: Dordrecht, 1981.

(33) Kuchitsu, K.; Morino, Y. *Bull. Chem. Soc. Jpn.* **1965**, *38*, 814.

(34) Dai, Q.; Hu, J.; Salmeron, M. *J. Phys. Chem. B* **1997**, *101*, 1994.

(35) Peters, S. J.; Ewing, G. E. *J. Phys. Chem. B* **1997**, *101* (50), 10880.

(36) Peters, S. J.; Ewing, G. E. *Langmuir* **1997**, *13* (24), 6345.

(37) Laux, J. M.; Fister, T. F.; FinlaysonPitts, B. J.; Hemminger, J. C. *J. Phys. Chem.* **1996**, *100* (51), 19891.

(38) Luna, M.; Rieutord, F.; Melman, N. A.; Dai, Q.; Salmeron, M. *J. Phys. Chem. A* **1998**, *102* (34), 6793.

(39) Dai, Q.; Hu, J.; Freedman, A.; Robinson, G. N.; Salmeron, M. *J. Phys. Chem.* **1996**, *100* (1), 9.

(40) Trakhtenberg, S.; Naaman, R.; Cohen, S. R.; Benjamin, I. *J. Phys. Chem. B* **1997**, *101* (26), 5172.

(41) Hu, J.; Xiao, X. D.; Ogletree, D. F.; Salmeron, M. *Science* **1995**, *268*, 267.

(42) Foley, N. J.; Thomas, K. M.; Forshaw, P. L.; Stanton, D.; Norman, P. R. *Langmuir* **1997**, *13* (7), 2083.

(43) Muller, E. A.; Rull, L. F.; Vega, L. F.; Gubbins, K. E. *J. Phys. Chem.* **1996**, *100* (4), 1189.

(44) Andrea, M. O.; Crutzen, P. J. *Science* **1997**, *276*, 1052.

(45) Charlson, R. J.; Schwartz, S. E.; Hales, J. M.; Cess, R. D.; Coakley, J. A.; Hansen, J. E.; Hoffman, D. J. *Science* **1992**, *255* (423−430).

(46) Crutzen, P. J. Composition, Chemistry and Climate of the Atmosphere. In *Air Pollution, Air Chemistry and Global Change*; Singh, H. B., Ed.; Von Nostrand Reinhold: New York, 1993.

(47) Lelieveld, J.; Crutzen, P. J. *J. Atmos. Chem.* **1991**, *12*, 229.

(48) Kaufman, Y. J.; Fraser, R. S. *Science* **1997**, *277* (5332), 1636.

(49) Murphy, D. M.; Thomson, D. S. *J. Geophys. Res.* **1997**, *102* (D5), 6353.

(50) Murphy, D. M.; Thomson, D. S.; Mahoney, T. M. J. *Science* **1998**, *282* (5394), 1664.

(51) Middlebrook, A. M.; Murphy, D. M.; Thomson, D. S. *J. Geophys. Res.* **1998**, *103* (D13), 16475.

(52) Novakov, T.; Penner, J. E. *Nature* **1993**, *365*, 823.

(53) Cruz, C. N.; Pandis, S. N. *J. Geophys. Res.* **1998**, *103* (D11), 13111.

(54) Ellison, G. B.; Tuck, A. F.; Vaida, V. *J. Geophys. Res.* **1999**, *104* (D9), 11633.

(55) Mozurkewich, M. *Geophys. Res. Lett.* **1997**, *24* (24), 3209.

(56) Kamens, R.; Odum, J.; Fan, Z. H. *Environ. Sci. Technol.* **1995**, *29* (1), 43.

(57) Liang, C. K.; Pankow, J. F. *Environ. Sci. Technol.* **1996**, *30* (9), 2800.

(58) Liang, C. K.; Pankow, J. F.; Odum, J. R.; Seinfeld, J. H. *Environ. Sci. Technol.* **1997**, *31* (11), 3086.